Journal of Nuclear Materials 545 (2021) 152614

Contents lists available at ScienceDirect

Journal of Nuclear Materials

journal homepage: www.elsevier.com/locate/jnucmat

Effect of irradiation on the stability of the corrosion layer produced in EUROFER by contact with lithium ceramics

T. Hernández [a,*], F.J. Sánchez [a], A. Moroño [a], M. Aristu [b], J.F. Marco [b]

[a] National Laboratory for Magnetic Fusion. CIEMAT. Avda. Complutense 40, 28040 Madrid, Spain
[b] Instituto de Química Física "Rocasolano", CSIC. Serrano 119, 28006 Madrid, Spain

ARTICLE INFO

Article history:
Received 2 June 2020
Revised 16 September 2020
Accepted 18 October 2020
Available online 22 October 2020

Keywords:
Eurofer
Corrosion
solid breeders
He/H_2O environment
tritium traps
Irradiation

ABSTRACT

This paper is concerned with the identification of the corrosive phase formed on the surface of low-activation steel Eurofer by contact with a ceramic bleeder and the effect of irradiation on the stability of the phase.

Tests were carried out at 550°C for 164 hours in a mixture of He/H_2O (99.8/0.2 %vol) for simulating the purge gas. The results show an important interaction of the steel with the lithium ceramic breeder. The corrosion layer was characterized by scanning electron microscopy, x-ray diffraction, secondary ion mass spectroscopy and Mössbauer spectroscopy to verify the oxides formed during the corrosion test and the modification of the containing species after being subjected to different doses of ionizing radiation and / or deuterium absorption. The relationship of the different iron states and high energy traps for hydrogen isotopes (deuterium) that could be generated in a corrosion layer during reactor operation was also established.

The results indicates that ionizing radiation up to the studied doses (200 MGy) does not produce additional defects to those generated by the transformation of hematite into non-stoichiometric wüstite, which is the fundamental compound of the corrosion layer by environmental deuterium.

1. Introduction

The solid breeder blanket concept allows having a lithium-containing tritium breeder as a non-mobile to reduce lithium and tritium inventory. Some advantages like the selection of a coolant that avoids problems related to safety and corrosion are expected. In the helium cooled Li-ceramics breeder concept, beryllium (as pebble bed) will be used for neutron multiplication and a lithium-ceramic is considered for the tritium breeding. A helium purge at low pressure is necessary for removing tritium through the porous ceramic breeder itself, while high pressure helium cooling goes through the first wall.

The compatibility of Reduced Activation Ferritic/Martensitic steels (RAFM) with liquid Li and Li-Pb has been studied in depth; however, little attention has been paid to the corrosion that may occur in case of low activation steels in contact with ceramic breeders, although it is proven that a corrosion layer is produced due to the oxidation of the surface by reaction in solid state between the steel and the pebbles containing lithium [1,2], as it has been reported previously [3-5]. Oxidation occurs at the interface and a product layer is formed which separates the reactants. As a result, subsequent reaction requires mass transport through the product layer. Numerous mechanisms of reaction have been considered to account for the many temperature-dependent oxidation phenomena observed. The many models differ in their assumptions about the rate-determining process: the transport mechanism through the oxide film, the driving forces of these transport mechanisms, etc. In general, for a particular metal, the oxidation mechanism will be a function of surface characteristics of the sample, temperature and elapsed time of reaction.

In this case, the corrosion layer has different characteristics from bare steel and therefore the absorption of tritium during reactor operation can vary, especially taking into account the effect of irradiation on ionic materials [6,7]. It is known that, depending on the dose, structural changes such as phase transformations or defects generation that act as high-energy traps for the tritium dispersed in the environment during operation may occur, which would make tritium release difficult.

In the past, the reference pebbles made of lithium orthosilicate or lithium metatitanate were considered as a pebble bed, however the last trend consists in using mixed breeder pebbles based on

* Corresponding author.
E-mail address: terea.hernandez@ciemat.es (T. Hernández).

https://doi.org/10.1016/j.jnucmat.2020.152614
0022-3115/

Li_4SiO_4 with additions of Li_2TiO_3 in different proportions in order to combine a sufficiently high lithium content and mechanical stability. This new generation of pebbles is considered as "advanced solid breeders" and was developed at the Karlsruhe Institute of Technology (KIT) by the KALOS process [8].

The aim of this work is to study the effects of ionizing irradiation and deuterium exposure on the corrosion layer produced by direct contact between ceramic pebbles and Eurofer. It also tries to establish the importance of such effect in terms of deuterium traps generated.

The robustness of the method used in this work against controlled parameter variation (temperature, composition, etc. allow the validation of results through objective evidence. Thus, the experimental results were checked by different methods; for example, the measurement of the corrosion layer and its composition was studied using the SEM-EDX and SIMS techniques in parallel. Dose measurement was carried out using standard coloration dosimeters and checked by optical absorption, and crystalline phases were monitored by Mossbauer and XRD.

2. Materials and methods

The reduced activation steel used in the experiments was Eurofer. Before being subjected to the corrosion test, the surface of the eurofer samples was sanded with 1200 um SiC paper to simulate the actual finish of the pieces. Specimens ($7 \times 7 \times 4$ mm^3) were kept in direct contact with the ceramic pebbles, in a special cylindrical chamber with a modular design manufactured at CIEMAT described in reference [4]. Chamber inner walls are covered with ZrO_2 for protection against corrosion. A purge gas flow of ~ $1cm^3$/min is maintained through chamber, which is controlled by a screw flowmeter. The chamber is introduced in a tubular furnace that permits testing temperatures up to 1500 °C. KST pebbles were a mixture of lithium silicate and titanate prepared in KIT by the KALOS method. The corrosion test was carried out at 550°C for 164 hours using a mixture of He/H_2O (99.8/0.2 % vol) flowing gas to simulate the purge gas.

The corrosion layer formed after the tests has been studied by scanning electron microscopy/Energy-dispersive X-ray spectroscopy (SEM / EDX) (Zeiss Auriga Compact/Bruker XFlash). Light ions (as D or Li) were analyzed by SIMS. This facility includes a Hiden MAXIM quadrupole mass analyzer and a Hiden IG-20 O_2 or Ar gas primary ion gun. SIMS analyses were carried out using a current up to 500 nA after confirming that it was enough to get through the coating and reach the base material.

XRD using the 2.5° grazing angle mode was used to determine the crystalline nature of the corrosion layer. The equipment used was PANalytical mod. X'Pert PRO MRD.

A confocal microscopy and interferometry system was used to study the topography of the corrosion layers and obtain 3D images. The equipment used was a Leica DCM8.

For irradiation with electrons, a Van der Graaff accelerator with 1.8 MeV was used until a dose of 200 MGy was reached. Irradiation with gamma rays was carried out in the Nayade facility of CIEMAT with ^{60}Co sources up to a dose of 10 MGy. Both irradiations were performed at room temperature.

After the irradiation the samples were kept in a deuterium atmosphere (99.8/D/0.2%H) at 350°C for 72 hours to allow the corrosion layers to absorb the gas. Then, thermal desorption was carried out by heating and identifying the species emitted by mass spectroscopy.

Conversion Electron Mössbauer (CEMS) spectra were recorded from the samples described in Table 1 using a constant acceleration spectrometer, a $^{57}Co(Rh)$ source and a parallel plate avalanche counter [9]. The velocity scale was calibrated using a metallic iron foil 6 μm thick. All the spectra were computer-fitted using Lorentzian-line profiles and the isomer shifts were referred to the centroid of the spectrum of α-Fe at room temperature.

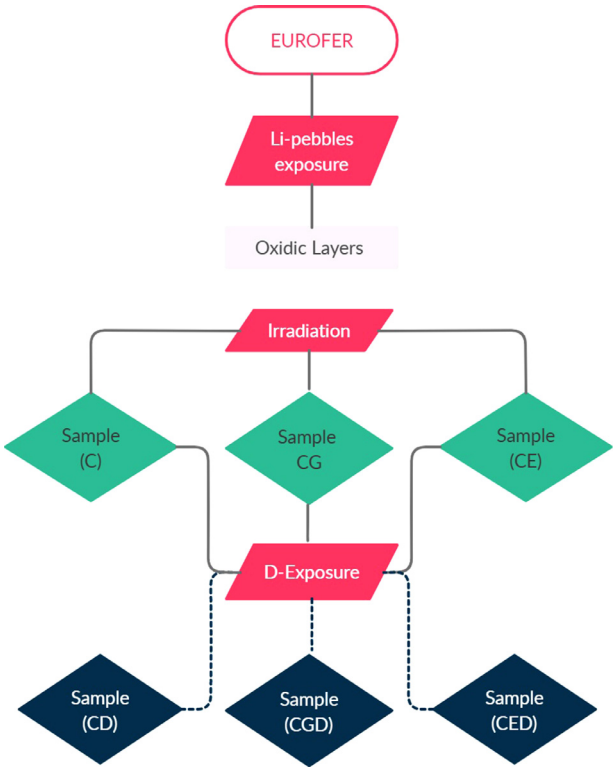

Fig. 1. Flow chart of the experiments carried out.

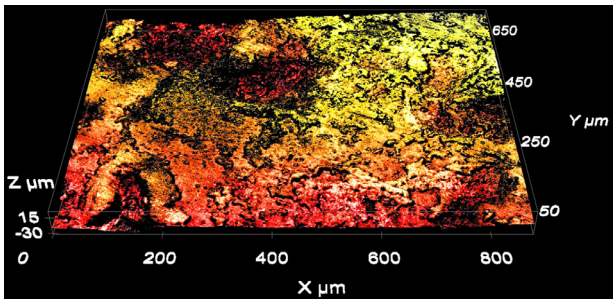

Fig. 2. Appearance of the surface of the Eurofer after the corrosion test. the color scale is related to the height.

The set of treatments and tests is shown in Fig. 1

3. Results

Fig. 2 shows the appearance of the surface of Eurofer after the corrosion test with the lithium pebbles. The different shades of color represent height, with reddish ones being the lowest and greenish ones being the highest. The original smooth surface of the steel has been transformed as a result of the oxidation process suffered. An adherent oxide layer can be observed that exhibits a roughness in absolute terms greater than 5 microns (peak-valley differences). It is interesting to take this consideration into account when talking about gas absorption, since it is favored on rough surfaces. Some "craters" are present due to the footprints left by the pebbles next to higher areas.

By grazing angle-XRD (Fig. 3), it is possible to identify the crystalline phases that have been formed by oxidation of the area exposed to the pebbles. The diffraction patterns show a mixture of hematite and lithium ferrite. Given the high diffusion capacity of

Table 1
Description of the samples.

Sample (C): Corrosion at 550°C and He/H2O.
Sample (CD): Corrosion at 550°C and He/H2O + D absorption.
Sample (CE): Corrosion at 550°C and He/H2O + e- irradiation (200 MGy)
Sample (CED): Corrosion at 550°C and He/H2O + e- irradiation (200 MGy)+ D absorption.
Sample (CG): Corrosion at 550°C and He/H2O + γ irradiation (10 MGy)
Sample (CGD): Corrosion at 550°C and He/H2O + γ irradiation (10 MGy)+ D absorption

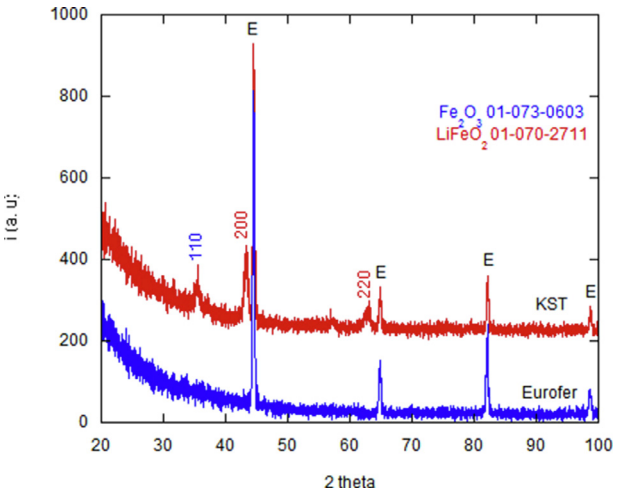

Fig. 3. Determination of phases by grazing angle XRD in sample CED (red pattern) in comparison with untrated Eurofer (blue pattern).

lithium ions also it is possible to find $LiFeO_2$ in which Li atoms occupy partially and randomly the octahedral sites in a cubic close packing of oxygen atoms of FeO with NaCl structure.

Fig. 4 provides the SEM cross section of the corrosion layer, as well as the basic chemical analysis obtained by EDX. After 10 days at 550°C in contact with pebbles, the corrosion layer is less than 1 micron thick. The analysis also provides information about its composition. The oxide is not homogeneous but is enriched in chromium close to Eurofer, while the outer zone is formed only by iron oxide. At the beginning of the corrosion process, a thin layer of chromium/iron mixed oxide is formed on the Eurofer surface. As the corrosion layer grows, Fe and Cr ions diffuse outward through the interphase. At that time, the diffusion rate of Fe ions is higher than that of Cr ions, so an iron oxide phase is formed on the outer side.

It is also possible to intuit pebble remains in the outermost area. The pattern shown in Fig. 4 is repeated all over the corroded surface; however, important variations in thicknesses were found.

In order to separate the effects produced in the corrosion layer by ionizing radiation or deuterium implantation, Mossbauer spectroscopy was used in the samples described in Table 1.

The room temperature CEMS spectra recorded from the different samples are depicted in Fig. 5. The corresponding hyperfine parameters obtained from the fit of such spectra are collected in Table 2.

The Mössbauer spectrum recorded from sample C is composed by an intense central paramagnetic doublet and various magnetic contributions (Fig. 5). The spectrum was fitted to one doublet and three sextets. The corresponding hyperfine parameters and the different spectral areas are collected in Table 2. The isomer shift and quadrupole splitting of the doublet are very close to that shown by $LiFeO_2$ [10]. Those parameters are also very similar to those characteristic of some Fe^{3+} oxyhydroxides, for example, lepidocrocite (γ-FeOOH) [11], which is one of the usual corrosion products of iron. However, given that the XRD data have proven the presence of

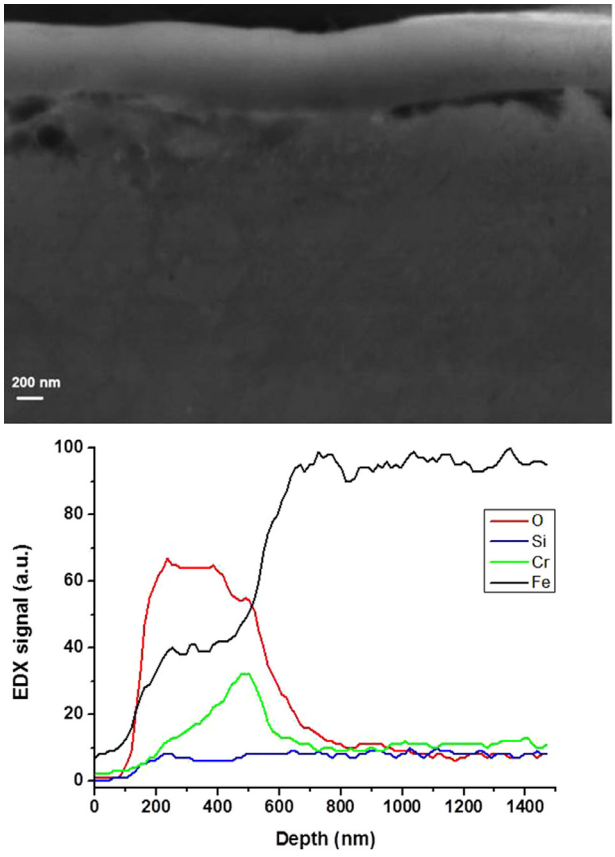

Fig. 4. Cross section and EDX composition of thecorrosion layer after 168 hours at 550°C in He/H_2O (up) and the corresponding EDX analisys (down).

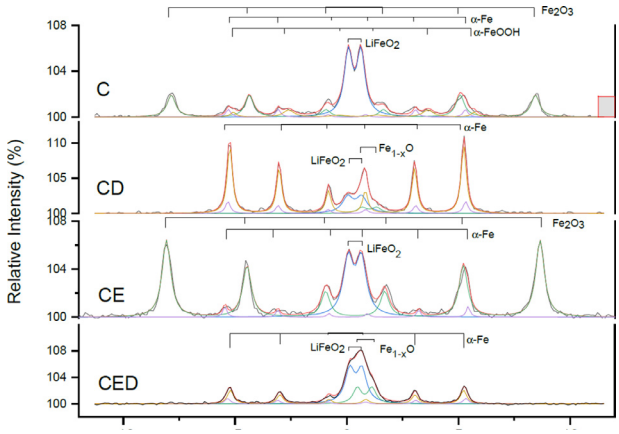

Fig. 5. CEMS spectra recorded from the samples C, CD, CE and CDE from top to botton.

Table 2
Hyperfine parameters obtained from the fitted spectra shown in Fig. 5 and their assignment to different chemical species.

Sample	Phase		H (T)	δ (mm / s)	2ε (mm / s)	Δ (mm / s)	Arearel (%)
C*	Lithium Iron (III) Oxide	$LiFeO_2$		0.35		0.57	44
	Ferric Oxide	Fe2O3	50.5	0.32	-0.06		38
	Goethite	α-FeOOH	33.4	0.41	-0.20		11
	Ferrite	α-Fe	32.9	0.00	0.00		7
CD*	Lithium Iron (III) Oxide	$LiFeO_2$		0.35		0.63	16
	Wüstite	Fe1-xO		1.00		0.65	5
	Ferrite	α-Fe	33.0	0.00	0.00		11
	Ferrite	α-Fe	32.5	0.00	0.00		67
CE*	Lithium Iron (III) Oxide	$LiFeO_2$		0.35		0.59	28
	Ferric Oxide	Fe2O3	51.9	0.33	-0.08		68
	Ferrite	α-Fe	33.8	0.00	0.00		4
CED*	Lithium Iron (III) Oxide	$LiFeO_2$		0.40		0.54	46
	Wüstite	Fe1-xO		0.80		0.66	19
	Ferrite	α-Fe	33.1	0.00	0.00		9
	Ferrite	α-Fe	32.3	0.00	0.00		26

H: Magnetic hyperfine field; $\boldsymbol{\delta}$: Isomer shift; $2\boldsymbol{\varepsilon}$: Quadrupole shift; $\boldsymbol{\Delta}$: Quadrupole splitting; **Arearel**: Relative area.

$LiFeO_2$, we think more likely to assign the doublet to such lithium-containing iron oxide. The various sextets can be assigned to ferrite (α-Fe), goethite (α-FeOOH) [12], and ferric oxide (Fe_2O_3). The hyperfine parameters of the sextet assigned to "ferric oxide" are not the canonical parameters expected for hematite [12] (which was identified by XRD), particularly as the isomer and quadrupole shifts is concerned (0.37 mms^{-1} and -0.22 mms^{-1}, respectively [12]). However, it is known [12] that the parameters can show variations similar to those observed here due to the occurrence of structural defects and/or inclusion of OH groups in the hematite crystal structure. In this context, it seems more appropriate to refer to such materials as hematite-like oxides [13]. Another remarkable fact is that the hyperfine magnetic field of the sextet assigned to goethite (32.7 T) is lower than that expected for bulk goethite (38.0 T). This reduction in the value of the hyperfine magnetic field, together with the large linewidth, is indicative of the presence of small particle/low crystallinity goethite [12] (and this can explain, then, why it has gone undetected in the X-ray diffractograms). The results indicate that the three Fe^{3+} species are the components of the corrosion layer while the ferrite contribution comes from the metallic substrate.

At this point it is interesting to consider the CEMS spectrum of sample CE that has been subjected to the same treatment than sample C followed by a subsequent electron irradiation at a dose of 200 MGy. Such spectrum only contains $LiFeO_2$ and Fe_2O_3 contributions, together with a small ferrite component, and no goethite is observed (we will come back to this point later).

Contrarily to this, the most intense contribution to the Mössbauer spectrum recorded from sample CD corresponds to two ferrite sextets arising from the metallic substrate (78%). We have used two sextets to fit the intense magnetic component observed in the spectrum because it gave a much better fit. The hyperfine parameters of these two sextets are very similar, except for the hyperfine magnetic fields (see Table 2). This can be interpreted in terms of iron environments in the Eurofer having different number of chromium atoms and/or to the occurrence of structural defects, which give place to components with slightly different hyperfine magnetic fields. The central paramagnetic doublets correspond to the corrosion products formed under these specific corrosion conditions (Table 1) and they can be assigned to $LiFeO_2$ (16%) and non-stoichiometric wüstite ($Fe_{1-x}O$) (5%) [13].

The Mössbauer spectrum recorded from sample CED is qualitatively comparable with that recorded from sample CD (it contains the same chemical species), the differences being due to their very different respective spectral areas. In the case of sample CED the ferrite contribution from the metallic substrate amounts to 35 % while those corresponding to $LiFeO_2$ and non-stoichiometric wüstite are 46% and 19%, respectively.

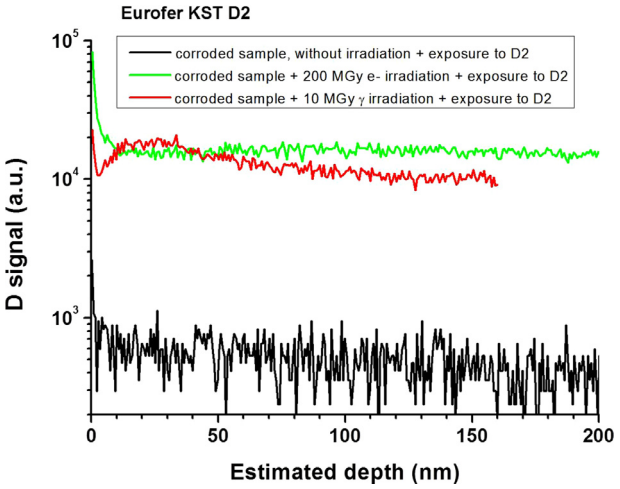

Fig. 6. Deuterium profiles obtained by SIMS for the CED and CGD samples compared to an unirradiated sample. for different samples.

Once the species that compose the corrosion layers are known, it is possible to obtain more information about them from the SIMS spectra that allow the identification of light elements such as deuterium. Fig. 6 compares the ability of irradiated samples to absorb deuterium as a function of radiation dose. Thus, the profiles for two samples exposed to deuterium previously irradiated at two different doses 10 and 200 MGy (samples CED and CGD with their corresponding baselines (samples CE and CG are presented. The difference between the two types of irradiation in terms of interaction with the material is penetration. In the case of the 1.8 MeV electron irradiation the penetration is about 1 mm in steel, but here the corrosion layer was irradiated directly and it is much thinner (micrometeres) than the electron penetration so it is assured that the corrosion layer is fully irradiated for both gamma and electron irradiation.

The Figure clearly shows that at low doses (10 MGy) deuterium is preferentially located on the outer surface and has a maximum before 50 nm. However, when the irradiation dose is increased, the distribution of deuterium appears homogeneously distributed over a much greater range.

On the other hand, thermal desorption provides information on the traps in which absorbed deuterium is located. Fig. 7 shows the

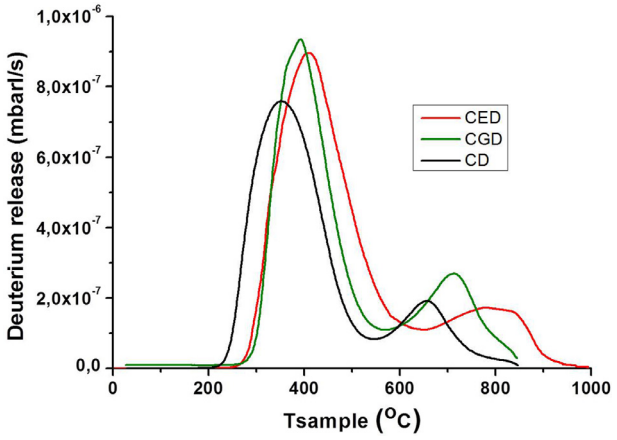

Fig. 7. Thermal desorption spectra obtained for different doses compared to an unirradiated sample.

results obtained for samples CED and CGD in relation to sample CD that was not irradiated. Given the dispersion inherent in the technique, the three spectra shown in the figure can be considered equivalent. Literature depicted that the low temperature band corresponds to defects of the Eurofer [14], while the high temperature band (about 800°C) could be related to accommodation traps in the corrosion layer. It is in this that a slight modification can be seen for the highest dose (200 MGy). The original band has widened and seems to be performed with a sequence of defects with very similar associated energies.

4. Discussion

In previous paper [15], it was shown that the corrosion layer formed on the Eurofer is not due solely to the reaction in the solid state between the pebble and the steel, but that in the presence of the He / H_2O mixture, a gaseous $Li_2O(H)$-type species are generated with high corrosion capacity. This flow surrounds the material, so the composition of the corrosion layer is similar regardless of whether there is contact or not, although thickness and roughness can vary.

It is well-known [16], that in an integral Conversion Electron Mössbauer spectrum (where all the electrons reemitted from the sample after the nuclear resonant absorption are collected irrespectively of their energy) the characteristic depth explored is approximately 300 nm although weighted to the uppermost 50 nm. Therefore, the presence and intensity of the ferrite contribution can be taken as a qualitative indication of the thickness of the corrosion layer formed on the Eurofer. It is clear from Fig. 5 that the most intense contribution from the Eurofer substrate corresponds to sample CD, i.e., the corrosion scale formed under these corrosion conditions is the thinnest of all the set of studied samples. Applying the same reasoning to all the spectra the thickness of the corrosion layer would increase in the order: sample CD<sample CED<sample C<sample CE. As it has been mentioned in the description of the microscopy results, although the exposition of Eurofer to the Li-containing pebbles gives place to relatively homogeneous oxidic layers from the compositional point of view, there exist important differences regarding the thickness of these layers. We assume, then, that the differences observed in Mössbauer spectroscopy in the thickness of the layers examined result from the dispersion in the thickness of the original oxidic layers and that they do not result from the subsequent treatments they have been subjected to. Therefore in the following discussion we will focus only on the chemical transformations induced in the oxidic layers by the exposition to deuterium and/or irradiation treatments.

According to the Mössbauer results, the exposition of Eurofer to the Li pebbles (sample C) results in the formation of a quite thick layer of corrosion products which is composed by various Fe^{3+}-containing compounds. Since the samples have been subjected for long hours to the flux of a gas containing a small percentage of water vapor, the formation of a minor amount of goethite appears to be plausible. The spectrum recorded from sample CE, i.e. from an original oxidic layer (OL) irradiated with a 200 MGy electron dose and without exposition to deuterium, does not show the chemical reduction of the initially present Fe^{3+} but the disappearance of the goethite contribution. At this respect is worth mentioning that it is known from very long [17] that the dehydration of goethite results in the formation of hematite and that this dehydration can be induced by electron irradiation through the local heating brought about by the impinging electron beam. This would explain the increase in the relative contribution of hematite to the spectrum of sample CE respect to that observed in the spectrum of sample C.

The situation in the presence of D is very different and may be related to the great capacity of $LiFeO_2$ to exchange of lithium for hydrogen, a fact that has been widely studied in batteries [18]. Thus the spectrum obtained for the CD sample is completely different. Here there is no hematite contribution and it contains a significant amount of Fe^{2+} in the form of non-stoichiometric wüstite. If we do not take into account the intense ferrite contribution to this sample we obtain that the corrosion layer contains 76% Fe^{3+} (in the form of $LiFeO_2$) and a 24% Fe^{2+} (in the form of non-stoichiometric wüstite). So, it is clear that the exposition to deuterium results in the partial reduction of the Fe^{3+} initially contained in the oxidic layer.

The spectrum recorded from sample CED (subjected to deuterium exposition and electron irradiation) only contains, as far as the corrosion layer is concerned, $LiFeO_2$ and non-stoichiometric wüstite (71% and 29%, respectively). So, in principle, and compared with sample CD, it would appear that the concomitant treatment involving electron irradiation and deuterium exposition would produce a slighter amount of Fe^{2+}-containing compounds (28% in sample CED against 24% in sample CD). However, given the very large ferrite contribution to the spectrum of sample CD, whose sextet overlaps strongly with the wüstite doublet, this latter statement should be taken with caution as the determination of the wüstite spectral area in the case of sample CD is subjected to a large uncertainty.

These results corroborate those obtained by thermal absorption shown in Fig. 7. The small variation found in sample CED with respect to CD for high temperature traps could justify different Fe^{2+}/Fe^{3+} content found in both samples, although it is so small that it rather suggests a wider transition range of states between Fe^{2+} and Fe^{3+}.

It has been reported [19] that the oxidation of thin films containing Fe_3O_4 islands on a FeO wetting layer results in the transformation of Fe_3O_4 into maghemite (γ-Fe_2O_3), both crystalizing in a spinel-related structure, and in the transformation of FeO into hematite. The mechanism of this latter transformation is explained in detail in ref [18]. Thus, it is plausible to think that the formation of FeO in the corrosion layers results from the reduction of hematite.

So, Mössbauer and TDS results indicate that high dose electron irradiation do not bring about the chemical reduction of the OL formed after Li pebble exposure and only if the samples are exposed to deuterium, a partial reduction of the original Fe^{3+}contained in the OL to $Fe^{2+}$is achieved.

5. Conclusions

Of all the samples studied, the one that is closest to the working conditions in the breeder blanket within the HCPB concept is

CED sample, that is, the one that contains a corrosion layer formed by direct contact of the Eurofer with the lithium pebbles, irradiation and an atmosphere rich in tritium (simulated in this paper with deuterium).

The most interesting conclusion of this study is that ionizing radiation up to the studied doses (200 MGy) does not produce additional defects to those generated by the transformation of hematite into non-stoichiometric wüstite, which is the fundamental compound of the corrosion layer by environmental deuterium. According to the results obtained by TDS, the effect of a high dose of radiation produces the homogenization of the positions that can house deuterium. This result is important in terms of the release of the Tritium. Although the operation temperature of blanket will be higher than 550°C, such temperature is correct for Eurofer, so, most of the tritium will be trapped and released simultaneously during the operation. However, a portion of tritium will be trapped in higher energy positions.

Attention should also be paid to the lithiation of the corrosion layer to form $LiFeO_2$. Lithium is a small ion with a great diffusion capacity and can reach the interface and penetrate the Eurofer through the impoverished Cr steel surface. The subsequent neutron bombardment would produce helium bubbles that would degrade the mechanical properties of the Eurofer.

Declaration of Competing Interest

None.

Acknowledgments

This work has been carried out within the framework of the EUROfusion Consortium and has received funding from the Euratom research and training programme 2014-2018 and 2019-2020 under grant agreement No 633053. “The views and opinions expressed herein do not necessarily reflect those of the European Commission." The authors acknowledge the funding by Spanish MICINN (project PID2019-105325RB-C31) and TechnoFusion Project (P2018/EMT-4437) of the CAM (Comunidad Autónoma de Madrid). Financial support from the Spanish Agencia Estatal de Investigación through project RTI2018-095303-B-C51 is also gratefully acknowledged. The authors wish to thank M. Martín, J.M. García, J. Valle and F. Jiménez for their help in the experiments.

Supplementary materials

Supplementary material associated with this article can be found, in the online version, at doi:10.1016/j.jnucmat.2020.152614.

References

[1] K. Mukai, F. Sánchez R. Knitter. Chemical compatibility study between ceramic breeder and EUROFER97 steel for HCPB-DEMO blanket. Journal of Nuclear Materials. 488. (2107) 196-203.
[2] M. Wang, M. Xiang, Y. Zhang, Z. Zhou, Study on the Chemical Compatibility Study Between Li_2TiO_3 Pebbles and 14Cr-ODS Steel, Journal of Fusion Energy 3 (2018) 247–254.
[3] O.K. Chopra, D.L. Smith, Interactions of solid ceramic breeding materials with structural alloys, Journal of Nuclear Materials 103 (1981) 555–560.
[4] T. Hernández, P. Fernández, R. Vila, Corrosion susceptibility of EUROFER97 in lithium ceramics breeders, Journal of Nuclear Materials 446 (2014) 117–123.
[5] K. Mukai, F. Sanchez, T. Hoshino, R. Knitter, Regina, Corrosion characteristics of reduced activation ferritic-martensitic steel EUROFER by Li 2 TiO 3 with excess Li, Nuclear Materials and Energy 15 (2018) (2018) 190–194.
[6] P.P. Seregin, F.S. Nasredinov, L.N. Vasilev, A study of radiation defects in solids by means of Mössbauer spectroscopy, Phys. Stat. Sol (a) 45 (1978) 11–16.
[7] Y. El Mendili, J.F. Bardeau, N. Randrianantoandro, J.M. Greneche, F. Grasset, Structural behavior of laser-irradiated γ-Fe2O3 nanocrystals dispersed in porous silica matrix : γ-Fe2O3 to α-Fe2O3 phase transition and formation of ε-Fe2O3, Sci Technol Adv Mater 17 (2016) 597–609.
[8] R. Knitter, M.H.H Kolb, U. Kaufmann, A.A. Goriaeb, Fabrication of modified lithium orthosilicate pebbles by addition of titania, Journal of Nuclear Materials 442 (2013) S433–S436.
[9] J.R. Gancedo, M. Gracia, J.F. Marco, Hyperfine Interactions 66 (1991) 83–93.
[10] M. Tabuchi, S. Tsutsui, C. Masquelier, R. Kanno, K. Ado, I. Matsubara, S. Nasu, H. Kageyama, Effect of cation arrangement on the magnetic properties of lithium ferrites (LiFeO2) prepared by hydrothermal reaction and post-annealing method, J. Solid State Chem. 140 (1998) 159–167.
[11] Chapter 3 R.E. Vandenberghe, E. De Grave, Application of Mössbauer spectroscopy in earth sciences, in: Y. Yoshida, G. Langouche (Eds.), Mössbauer Spectroscopy. Tutorial Book, Springer-Verlag, Berlin Heidelberg, 2013, pp. 91–186. Chapter 3.
[12] M.-Z. Dang, D.G. Rancourt, J.E. Dutrizac, G. Lamarche, R. Provencher, Interplay of surface conditions, particle size, stoichiometry, cell parameters, and magnetism in synthetic hematite-like materials, Hyperfine Interactions 117 (1998) 271–319.
[13] Chapter 12 E. Murad, J.H. Johnston, Iron Oxides and Oxyhydroxides, in: Gary J. Long (Ed.), Mössbauer Spectroscopy Applied to Inorganic Chemistry, 2, Plenum, New York, 1987, pp. 507–582. Chapter 12.
[14] K. Ono, M. Miyamoto, F. Kudo, Release of deuterium from irradiation damage in Fe–9Cr–2W ferritic alloy irradiated with deuterium ions, Journal of Nuclear Materials 452 (2014) 46–50.
[15] T. Hernández, M. CarmonaGázquez, M.Malo F.J.Sánchez, Corrosion mechanisms of Eurofer produced by lithium ceramics under fusion relevant conditions, Nuclear Materials and Energy 15 (2018) 110–114 May.
[16] Chapter 22 J.F Marco, J.R. Gancedo, M. Monti, J. de la Figuera, Mössbauer spectroscopy and surface analysis, in: Virender K. Sharma, Göstar Klingelhöfer, Tetsuaki Nishida (Eds.), Mössbauer Spectroscopy. Applications in Chemistry, Biology, and Nanotechnology, John Wiley & Sons, Inc., Hoboken, New Jersey, 2013, pp. 455–469. Chapter 22.
[17] C.J. Goss, The kinetics and reaction mechanism of the goethite to hematite transformation, Mineralogical Magazine 51 (1987) 437–451.
[18] A.R. Armstrong, D.W. Tee, F. La Mantia, P. Novák, P.G. Bruce, Synthesis of Tetrahedral LiFeO2 and Its Behavior as a Cathode in Rechargeable Lithium Batteries, J. Am. Chem. Soc. 130 (11) (2008) 3554–3559.
[19] Kevin F McCarty, M Monti, B Santos, A Mascaraque, O Rodriguez de la Fuente, MA Niño, TO Mentes, A Locatelli, JF Marco, J Figuera, Oxidation pathways in bi-component ultrathin Iron Oxide Films, The Journal of Physical Chemistry C 116 (21) (2015) 11539–11547.